Zhang *et al. Int J Concr Struct Mater* (2020) 14:10
https://doi.org/10.1186/s40069-019-0382-8

International Journal of Concrete Structures and Materials

RESEARCH Open Access

Research on the Corrosion/Permeability/Frost Resistance of Concrete by Experimental and Microscopic Mechanisms Under Different Water–Binder Ratios

Rongling Zhang[1,2*], Peng Liu[3*], Lina Ma[1*], Zijiang Yang[1], Huisu Chen[4], Han Xing Zhu[2], Huigang Xiao[5] and Jia Li[1,6]

Abstract

To study the influence of different water–binder ratios on the corrosion, permeability, and freezing properties of concrete, we produced different strengths of concrete with respective water–binder ratios of 0.32, 0.38, 0.50, and 0.66. The corrosion resistance of the concrete was studied via three corrosion methods: full immersion, half immersion, and dry and wet cycles. The impermeability and frost resistance of concrete with different water–binder ratios were tested and analyzed. The test results show that the corrosion modes in order from strong to weak were dry and wet cycles, half soaking, and full soaking. The relative dynamic elasticity modulus and freeze–thaw index were used to evaluate the frost resistance of concrete based on the analysis of three indices of frost resistance. To study the internal mechanism of corrosion of concrete with different water–binder ratios, microscopic pore structure testing of the concrete was conducted using a Micromeritics AutoPore IV 9500 Series instrument. The porosimeter studies show that the smaller the water–binder ratio, the more small pores and the denser the concrete. The smaller the water–binder ratio, the higher the strength and the better the corrosion, permeability, and frost resistance.

Keywords: corrosive environments, immersion method, service life, pore structure, mechanics

1 Introduction

Due to the different levels of importance of engineering structures and service life, the strength grades of concrete structures are also different in actual projects. Different strength grades of concrete directly affect the durability of concrete. The water–binder ratio is one of the most important factors to determine the strength of concrete. The actual structures are located in different environments. They are subject to different environmental influences, including corroding environments, freeze–thaw environments, etc. These different factors directly or indirectly affect the durability of concrete. The deterioration of concrete has been of great concern globally in recent decades. Research on the concrete deterioration mechanism in different environments has important implications for concrete design and prejudged service life. Some scholars have carried out research in this field (Haynes et al. 2008; Neville 2004; Rao et al. 2017). The strength of concrete increases in the early stages of corrosion and decreases gradually later (Zhang et al. 2018). A high-salinity environment thus has a significant effect on weakening the mechanical performance of concrete (Zanqun et al. 2016). Du et al. stated (2016) that concrete

*Correspondence: zhangrl@mail.lzjtu.cn; lop868@163.com; malina@mail.lzjtu.cn
[1] School of Civil Engineering, Lanzhou Jiaotong University, Lanzhou 730070, China
[3] School of Civil Engineering, Central South University, 22 Shaoshan Road, Changsha 410075, China
Full list of author information is available at the end of the article
Journal information: ISSN 1976-0485 / eISSN 2234-1315

with a lower water/cement (w/c) ratio always has a corresponding smaller corrosion layer thickness. Research results from Dehwah et al. (2002) showed that the rate of chloride-induced reinforcement corrosion in concrete specimens exposed to sodium chloride plus magnesium sulfate solutions was higher than that in concrete specimens exposed to sodium chloride plus sodium sulfate solutions. Exposure to sulfate is well known to affect the durability of concrete materials and, thus, concrete structures. Zhang et al. (2017) studied the degradation of calcium sulfoaluminate cement subjected to wet–dry cycles in sulfate solution. Research results from Yu et al. (2017) showed that the damage and deterioration of concrete under chemical attack are remarkably accelerated by salt crystallization. Shaheen and Pradhan (2017) determined that ordinary Portland cement performed better against Mg-oriented sulfate attack whereas Portland pozzolana cement performed better against Na-oriented sulfate attack in the presence of chloride ions. Najjar et al. (2017) showed that full immersion simulating chemical sulfate attack and partial immersion combined with cyclic temperature and relative humidity are conducive to physical salt attack. The results from Mahmoodian and Alani (2017) revealed that samples' overall mass increased at the early stages of the corrosion process, and the overall mass of the samples decreased significantly at the later stages of the testing process with respect to the acidity of the solutions used. Valencia Saavedra et al. (2016) suggested that it is necessary to evaluate the material's compressive strength loss to accurately characterize the performance of a concrete mixture exposed to an aggressive environment. Test results from Gao et al. (2013) showed that under alternate action of wet–dry cycling, concretes are attacked by expansive products such as ettringite and gypsum during the wetting cycle, and crystallization damage, induced by evaporation, is superposed during the drying cycle. Experimental results from Hai-long et al. (2012) showed that damage to concrete is caused by the expansion of chemical reaction products and crystallization of sodium sulfate under a sodium sulfate and wet–dry cycle environment. Liangxue et al. (2016) reported that the final strengths were only 82.84% and 90.22% in specimens which were kept in a normal environment and immersed in distilled water after aging for 360 days, respectively.Many studies have researched concrete expansion and cracking due to sulfate exposure (Aye and Oguchi 2011; Gao and Zou 2015; Rozière et al. 2009), but due to the different research objectives and the different test environments, different test schemes and evaluation indices have been selected to study the performance of concrete subjected to sulfate attack (El Maaddawy and Soudki 2007). Therefore, the research in this field is still in a chaotic state (Neville 2004), and there is no unified accepted knowledge system. How to improve the corrosion resistance of concrete structures is of great engineering significance. The concrete corrosion mechanism varies greatly under different sulfate conditions (Tulliani et al. 2002).

Highlights

- The influence mechanism of corrosion was determined by analyzing the microstructure of concrete.
- Experimental research on the corrosion/permeability/frost properties of concrete was carried out.
- The inner influence mechanism of corrosion/permeability/frost was determined by analyzing the microstructure.

2 Materials and Methods

2.1 Materials

The mechanical properties of the raw materials used to make the specimens were measured before any tests were performed. The silicate cement used contained 65.21% CaO, 4.3% Al_2O_3, 4.89% Fe_2O_3, 22.1% SiO_2, 0.012% chloride ions, and 0.43% alkali content. The fine aggregate was natural sand with a fineness modulus of 2.3, where the apparent density was 2608 kg/m^3. The index of firmness was 3.6%, the mud content was 1.7%, and the alkali aggregate reactivity was 0.13%. The coarse aggregate was broken basalt with particle sizes within the range of 5 mm to 10 mm; its alkali aggregate reactivity was 0.12%, and its apparent density was 2369 kg/m^3. The index of firmness was 3.6% and the mud content was 0.3%. The AN4000 polycarboxylic water reducer had a water reducing ratio of 26.0%, air content of 2.5%, bleeding rate of 4.0%, and shrinkage ratio of 72%. The AN1 air entraining agent had a water reducing ratio of 26.0%, air content of 2.4%, bleeding rate of 2.6%, and shrinkage ratio of 96%.

2.2 Experimental Design

Four types of concrete were tested in this experiment, and the details of the mixture proportions are listed in Table 1.

Seventy-two groups (3 blocks per group) of specimens with dimensions of $100 \times 100 \times 100$ mm (compressive strength test) and $40 \times 40 \times 160$ mm (flexural strength test) were cured for 1 day. Then, the prism specimens were demolded and cured in a standard curing room with a temperature of 20 ± 3 °C and relative humidity over 90% for 28 days. Then they were soaked in a strong corrosive solution and water with full immersion (I_F, Fig. 1a), half-immersion (I_H, Fig. 1b), or in dry–wet cycles (I_C, Fig. 2) for the three corrosion methods.

Twelve groups of prismoid specimens with dimensions of $100 \times 100 \times 400$ mm were cured for 24 days. Then the

Table 1 Mixture proportions of the specimens.

Type	Strength grade	W/C ratio %	Water kg/m^3	Cement kg/m^3	Fine aggregate kg/m^3	Coarse aggregate kg/m^3	Water reducer kg/m^3	Air entraining agent kg/m^3	Air content %
A-1	C50	0.32	150	465	764	1358	6.98	0.19	5.0
A-2	C40	0.38	167	440	568	927	6.60	0.15	5.5
A-3	C30	0.50	155	310	550	760	3.72	0.09	5.5
A-4	C20	0.66	190	288	545	694	1.73	0.12	5.6

freezing–thawing test was carried out after soaking in water at 20 ± 2 °C for 4 days. The frost resistance of the concrete was evaluated by the number of freeze–thaw cycles of concrete samples under the condition of water freezing and thawing.

Thirty-six groups of cylindrical specimens were cured for 24 ± 2 h. Their diameters were 100 mm and their heights were 50 mm. The prism specimens were demolded and cured in a standard curing room with a temperature of 20–25 °C for 28 days. The chloride penetration resistance of the concrete was determined by electric flux testing of the sample.

2.3 Test Method

The total salt content of the strongly corroding salt solution was 22.36%. The contents of sodium sulfate and magnesium chloride were 10.36% and 12.00%, respectively. In order to keep the concentration of the corrosive medium constant during the test, we changed the solution once every 50 days. During the immersion process, the sample was titrated with 1 N H_2SO_4 every day to neutralize the $Ca(OH)_2$ released by the sample in solution. The pH value of the solution was kept at about 7.0 by stirring while titrating. The cycle system of the dry and wet circulation method involved a drying time of 8 h and an immersion time of 15 h during the experiment. The dry and wet circulation system of the specimen was 15 h soaking plus 1 h cooling plus 8 h drying, and each cycle lasted 24 h.

Each freezing–thawing cycle was completed within 2–4 h, and the time for melting was not less than one-quarter of the whole freezing–thawing cycle time in the frost resistance test. The minimum and maximum temperatures of the specimen center should be controlled within 18° and 5°, respectively, during freezing and melting. The conversion time between freezing and melting was no more than 10 min.

The specimens were treated with vacuum and water retention before the electric flux test. The current value was measured periodically in an environment of 20–25 °C and the electric flux was calculated.

The requirements of test samples and test methods were chosen in accordance with the standard for test methods of long-term performance and durability of ordinary concrete (GB/T 50082-2009) (China 2009).

The corrosion resistant coefficient of flexural resistance and corrosion resistant coefficient of compression resistance for concrete can be calculated using Eqs. (1) to (7) (China 2009) as follows:

$$K_P = \frac{f_p}{f_p^w} \times 100\% \tag{1}$$

$$K_c = \frac{f_c}{f_c^w} \times 100\% \tag{2}$$

$$\Delta W_{ni} = \frac{w_{0i} - w_{ni}}{w_{0i}} \times 100\% \tag{3}$$

$$\Delta W_n = \frac{\sum_{i=1}^{3} \Delta W_{ni}}{3} \times 100\% \tag{4}$$

$$K_b = \frac{P \times N}{300} \tag{5}$$

$$Q = 900\ (I_0 + 2I_0 + 2I_{60} + \cdots + 2I_t + \cdots + 2I_{300} + 2I_{330} + 2I_{360}) \tag{6}$$

$$Q_s = Q_x \times (95/x)^2 \tag{7}$$

where K_p, K_c, ΔW_{ni}, ΔW_n, ΔK_b, Q, and Q_s are the corrosion resistant coefficient of flexural resistance and the corrosion resistant coefficient of compression resistance for concrete; the mass loss rate of the concrete specimen after N freeze–thaw cycles; the mass loss rate of a single specimen; the freeze–thaw index; the total electric flux through the specimen; and the electric flux through the specimens with a diameter of 95 mm, respectively. f_p and f_c are the flexural strength and compressive strength of the specimen at a certain age in the erosion solution, respectively. f_p^w and f_c^w are the flexural strength of

a I_F **b** I_H

Fig. 1 Specimens from full immersion and half immersion.

a 50 times **b** 100 times

Fig. 2 Appearance changes after dry–wet cycle erosion.

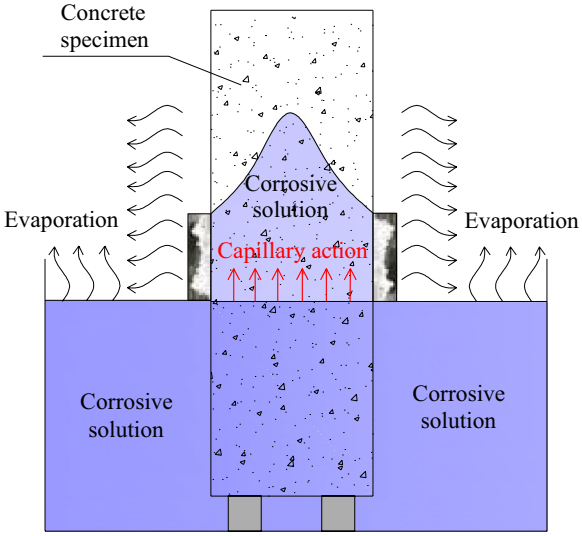

Fig. 3 Corrosion process of concrete.

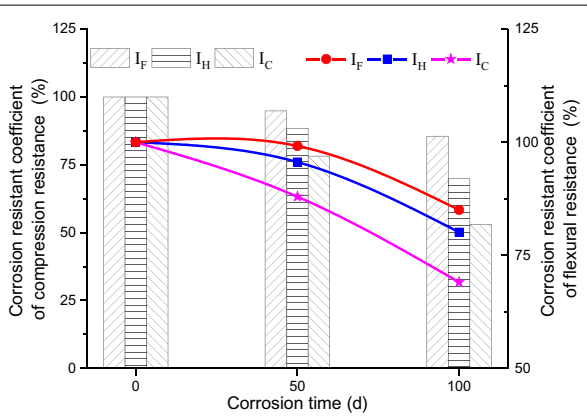

Fig. 4 Effect on strength of C20 concrete caused by three immersion methods.

concrete specimens compared with that of standard curing specimens in the age period of the sulphate corrosion specimens and the compressive strength of the concrete specimens compared with that of standard curing in the age period of the sulfate-corroded specimens, respectively. w_{ni} and w_{0i} are the mass of the ith concrete specimen after N freeze–thaw cycles and the quality of the ith concrete specimen before freeze–thaw cycle testing, respectively. N is the number of freeze–thaw cycles, and P is the relative dynamic elastic modulus of a set of concrete specimens after N freeze–thaw cycles. I_0 and I_t are the initial current and current at time t, respectively. Q is the flux through the specimen with diameter x.

The pore structures and interfacial properties of cement-based materials are influenced by the properties of ion transport behavior and durability (Cho 2012). The mercury intrusion method (MIP, Method of Mercury intrusion pore measurement) can be used to calculate pore size and the corresponding pore volume by the function of the amount of Mercury in concrete materials and the applied pressure. In order to study the influence mechanism of corrosion, the total porosity, specific surface area, and average pore diameter of the concrete microstructure were analyzed and compared.

Before exposure to sulfates, small pieces were retrieved from selected specimens to evaluate the pore size distribution using Mercury Intrusion Porosimetry (MIP) at the age of 28 days. The MIP measurements were performed using a Micromeritics AutoPore IV 9500 Series porosimeter and according to ASTM D4404 (Standard Test Method for Determination of Pore Volume and Pore Volume Distribution of Soil and Rock by Mercury Intrusion Porosimetry) (D4404 2010).

3 Durability Analysis of Test Results

3.1 Effect of Different Immersion Methods for Concrete in a Corrosive Environment

The immersion method is one of the most important factors in concrete corrosion. Different immersion methods result in different corrosion products. The effect on the compressive strength and flexural strength of concrete was analyzed under three immersion methods: half soaking, full soaking (typical corrosion method in actual structures, Fig. 3), and dry–wet circulation.

The strength test results are summarized in Fig. 4, and each bar indicates a certain corrosion method to make it easier to see the difference in the change of strength of concrete specimens with varied corrosion. The compressive strength and flexural strength of concrete decreased under the three immersion methods with continuous increase of corrosion time. The corrosion resistant coefficients of compression resistance at 50 days and 100 days were 0.99 times and 0.85 times that before corrosion in the full immersion test, respectively. The corrosion resistant coefficients of compression resistance at 50 days and 100 days were 0.95 times and 0.80 times that before corrosion in the half immersion test, respectively. The corrosion resistant coefficients of compression resistance at 50 days and 100 days were 0.88 times and 0.69 times that before corrosion in the full immersion test, respectively. The corrosion resistant coefficients of flexural resistance at 50 days and 100 days were 0.95 times and 0.86 times that before corrosion in the full immersion test, respectively. The corrosion resistant coefficients of flexural resistance at 50 days and 100 days were 0.88 times and 0.70 times that before corrosion in the half immersion test, respectively. The corrosion resistant coefficients of flexural resistance at 50 days and 100 days were 0.78 times and 0.53 times that before corrosion in the full immersion test, respectively. The research results showed that the full immersion corrosion was the weakest, half immersion corrosion was second, and dry–wet cycle corrosion was the strongest.

Figure 5 shows that the corrosion resistant coefficient of compression resistance and the corrosion resistant coefficient of flexural resistance were greater at 50 days when compared to those before corrosion. The corrosion resistant coefficients of compression resistance under full immersion, half immersion, and dry–wet cycles at 50 days were 1.05, 1.04, and 0.91 times that before corrosion, respectively. The corrosion resistant coefficients of flexural resistance under full immersion, half immersion, and dry–wet cycles were 1.00, 0.95, and 0.87 times that before corrosion, respectively. The rule was the same as in Fig. 4: the research results showed that the full immersion corrosion was the weakest, half immersion corrosion was second, and dry–wet cycle corrosion was the strongest. Figure 6 shows that the corrosion resistant coefficients of compression resistance and the corrosion resistant coefficients of flexural resistance at 50 days and 100 days were greater when compared to that before corrosion. The corrosion resistant coefficient tends to increase from 50 days to 100 days. The latter was dominant under the above conditions, and the corrosion resistant coefficient of compression resistance and corrosion resistant coefficient of flexural resistance were greater than those for C40 concrete.

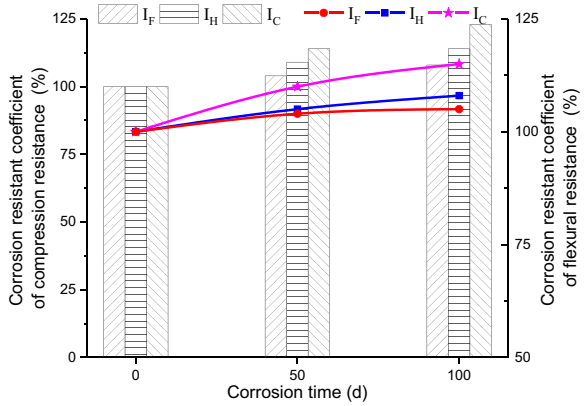

Fig. 6 Effect on strength of C40 concrete caused by three corrosion methods.

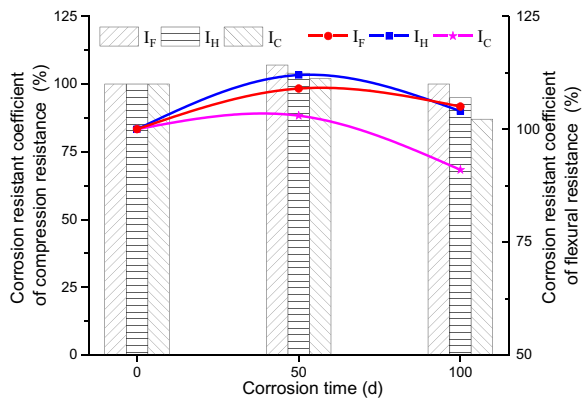

Fig. 5 Effect on strength of C30 concrete caused by three corrosion methods.

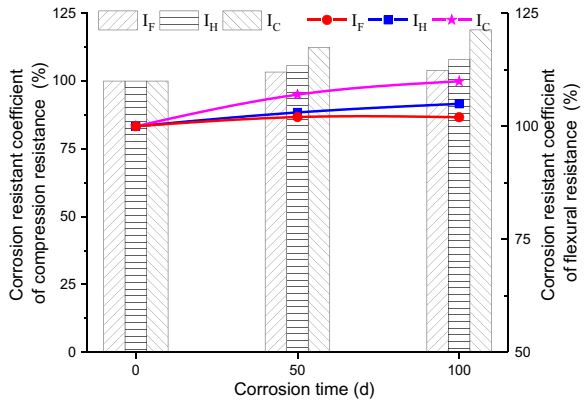

Fig. 7 Effect on strength of C50 concrete caused by three corrosion methods.

Figure 7 shows that the corrosion resistant coefficient of compression resistance and the corrosion resistant coefficient of flexural resistance at 50 days and 100 days were greater when compared to those before corrosion. The increase range of the corrosion resistant coefficient of compression resistance and the corrosion resistant coefficient of flexural resistance for IH was greater than that for IF during the process of corrosion from 50 days to 100 days under the three corrosion conditions. Similarly, the increase range for IC was larger than that for IH's corrosion resistant coefficient of compression resistance and corrosion resistant coefficient of flexural resistance. This shows that C50 concrete has good corrosion resistance.

$$Na_2SO_4 + 10H_2O \rightarrow Na_2SO_4 \cdot 10H_2O \quad (8)$$

$$Na_2SO_4 \cdot 10H_2O + Ca_2(OH)_2 \rightarrow Ca_2SO_4 \cdot 2H_2O + 2NaOH + 8H_2O \quad (9)$$

$$MgSO_4 + Ca_2(OH)_2 + 2H_2O \rightarrow Ca_2SO_4 \cdot 2H_2O + Na(OH)_2 \quad (10)$$

$$3Ca_2SO_4 \cdot 2H_2O + 4CaO \cdot Al_2O_3 \cdot 12H_2O + 14H_2O \rightarrow 3CaO \cdot Al_2O_3 \cdot 3Ca_2SO_4 \cdot 12H_2O + Ca_2(OH)_2 \quad (11)$$

During the sulfate resistance tests on the concrete specimens, sulfate ions infiltrate the concrete specimens and the sulfate stimulate the hydration of cementitious materials, transformation of anhydrous Na_2SO_4 to $Na_2SO_4{\cdot}10H_2O$ increases the volume by approximately 3.1 times, transformation of $Na_2SO_4{\cdot}10H_2O$ and $MgSO_4$ to $Ca_2SO_4{\cdot}2H_2O$ increases volume by approximately 2 times, and the reaction produced AFt (ettringite) increases volume by approximately 1.2 times., Also, at the early stage of the reaction, pores are filled with salt crystals that will enhance concrete strength. With continuing crystallization, the crystallization pressure will result in the non-uniform expansion of the concrete as the increasing formation of the hydrated products such as ettringite and gypsum filled the pores. Finally, the concrete cracks when the crystallization pressure exceeds the tensile strength of the concrete. Therefore, the concrete strength finally decreases by the simultaneous action of the physical and chemical corrosion caused in the salt formation process.

3.2 Effect of Different Strengths of Concrete in Corrosive Environments

The strength of concrete is another very important factor influencing the corrosion of concrete. Figure 8 shows the strength and corrosion resistance of different concrete strengths in a corrosive environment.

The corrosion resistant coefficient of compression resistance was less than 1 at 50 days and 100 days for C20 concrete, in Fig. 8a, and the compressive strength resistance coefficients of other strength grades of concrete were greater than 1 at 50 days and 100 days. The corrosion resistant coefficients of flexural resistance from C20 to C40 concrete were less than 1 at 50 days and 100 days, except for C50 concrete in Fig. 8a. The corrosion rules for different concrete strengths in Fig. 8b are the same as those in Fig. 8a. The corrosion resistant coefficient of compression resistance and corrosion

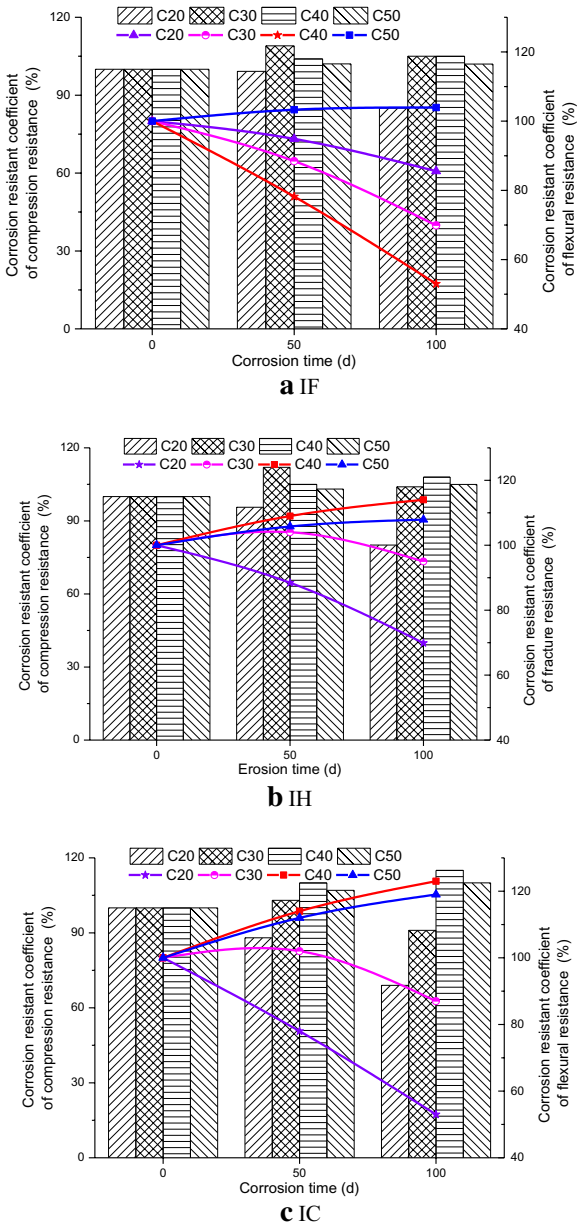

Fig. 8 Influence of concrete strength on corrosion.

resistant coefficient of flexural resistance were less than 1 at 50 days and 100 days for C20 concrete in Fig. 8c. The corrosion resistant coefficient of compression resistance and corrosion resistant coefficient of flexural resistance were greater than 1 when C30 concrete was corroded for 50 days,and the corrosion resistant coefficient of compression resistance and corrosion resistant coefficient of flexural resistance were less than 1 when the corrosion time reached 100 days. The corrosion resistant coefficient of compression resistance and corrosion resistant coefficient of flexural resistance were greater than 1 when the corrosion times of C40 and C50 concrete were 50 days and 100 days.

C20, C30, C40, C50 concrete specimens experienced dry and wet cycle corrosion for 50 days separately, then, the materials for XRD tests were obtained at 5 mm below the surface of those specimens (Fig. 9). According to the XRD analyses, the main substances in the tested concrete specimens were C–S–H, AFt, $Ca(OH)_2$, $CaCO_3$ and unhydrated cement particles. In addition, $CaSO_4{\cdot}2H_2O$ and $Mg(OH)_2$ are also observed. As the strength of the concrete decreases, the peak values of AFt, $CaSO_4$ and $Mg(OH)_2$ all increases. According to the above analysis, the higher the strength of concrete, the stronger the corrosion resistance. It can be seen from the data of the strength corrosion coefficient that the anti-corrosion performance of C40 and C50 concrete was better than that of C20 and C30 concrete. This suggests that the concrete design strength should not be lower than that of C40 under a corrosive environment.

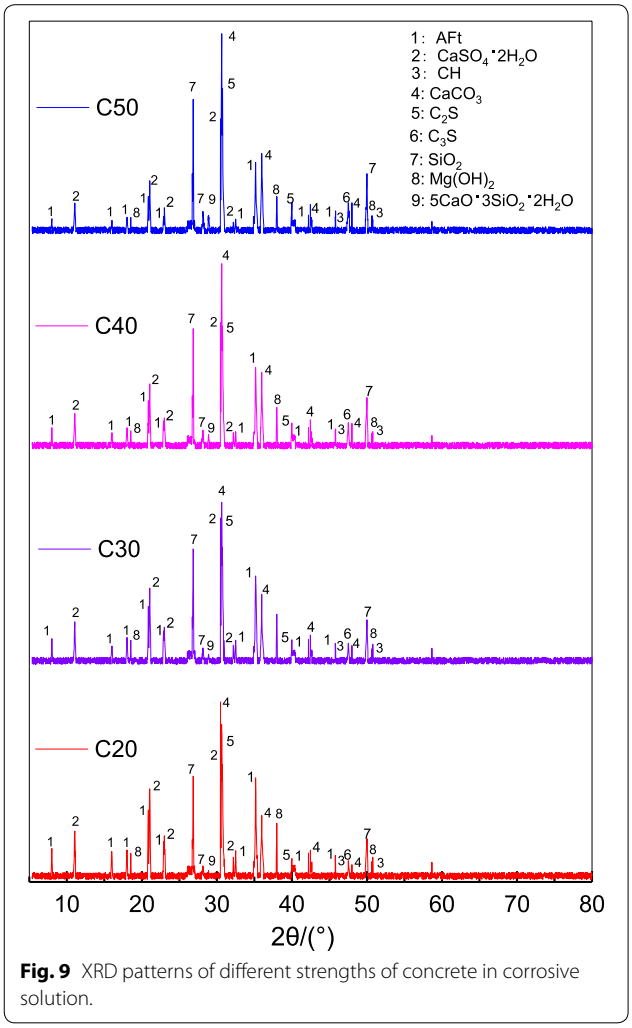

Fig. 9 XRD patterns of different strengths of concrete in corrosive solution.

3.3 Freezing Resistance of Concrete Under Different Water–Binder Ratios

Freezing resistance is a very important index of concrete durability. Via testing the relative dynamic elastic modules, mass loss, and freeze–thaw index, the influence law of concrete durability under different water–binder ratios was obtained. The analysis results are shown in Figs. 10, 11, and 12.

It can be seen from Fig. 10 that damage occurs in C20 concrete when 25 freeze–thaw cycle are completed, and the relative dynamic elastic modulus was only 19.06, which is very small. C30 concrete, C40 concrete, and C50 concrete can withstand up to 300 freezing–thawing cycles. As the number of freeze–thaw cycles increases, the relative dynamic elastic modulus of the concrete decreases. The relative dynamic elastic modulus of C40 concrete was 1.19 times that of C30 concrete at 300 freeze–thaw cycles. The relative dynamic elastic modulus of C50 concrete was 1.23 times that of C30 concrete at 300 freeze–thaw cycles. The relative dynamic elastic modulus of C50 concrete was only 1.03 times that of

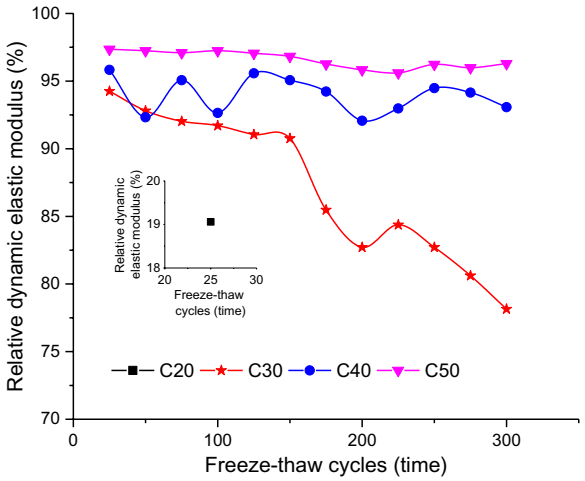

Fig. 10 Relative dynamic elastic modulus under freeze–thaw cycles.

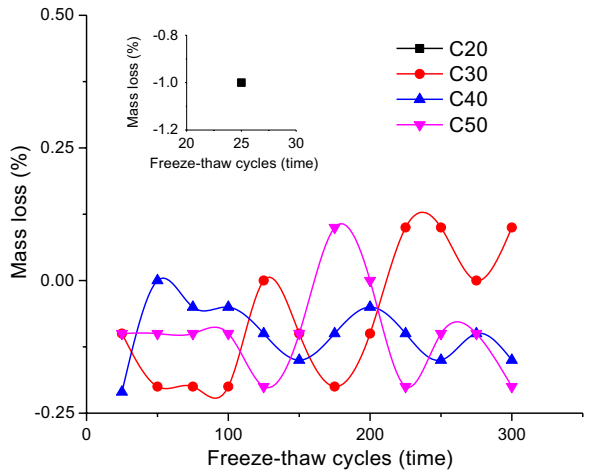

Fig. 11 Mass loss under freeze–thaw cycles.

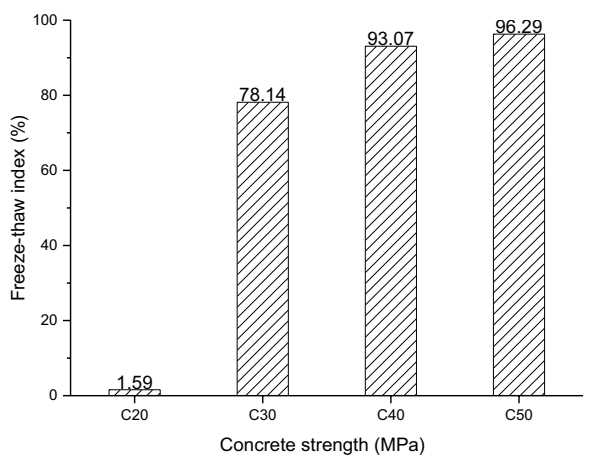

Fig. 12 Freeze–thaw indices of different strengths of concrete.

C40 concrete at 300 freeze–thaw cycles. The higher the strength of the concrete, the greater its relative dynamic elastic modulus.

Figure 11 shows that the mass loss from different concrete strengths was very small under freeze–thaw cycles. The mass loss range was 0.1 to −0.21, and the change rule was not obvious. The evaluation of the freezing resistance of concrete by mass loss was not obvious compared with the relative dynamic elastic modulus. Thus, the relative dynamic modulus of elasticity is recommended to evaluate the frost resistance of concrete.

It can be seen that the frost–thaw index was only 1.59% in the analysis of concrete strength grade and freeze–thaw resistance index in Fig. 12, and damage occurred after 25 cycles of freeze–thawing of C20 concrete. The freeze–thaw resistance indices of C40 concrete and C50 concrete were 1.19 times and 1.23 times that of C30 concrete, respectively. The higher the concrete strength, the higher the freezing and thawing index and the better the frost resistance. Improving concrete strength is an effective method to improve the frost resistance of concrete. However, when the concrete was improved to a certain extent, the improvement of frost resistance was not obvious. For example, the freeze–thaw resistance index of C40 concrete was 93.07, and that of C50 concrete was 96.29. The freeze–thaw resistance indices were very close. Therefore, it is advisable to select an appropriate concrete strength grade to meet the requirements of frost resistance and to meet the requirements of concrete durability.

3.4 Anti-permeability of Concrete Under Different Water–Binder Ratios

The impermeability of concrete is an important index that reflects the resistance of concrete to external material invasion. The electric flux is the current passing through the concrete sample and is used to judge the strength of anti-permeability performance.

Figure 13 shows that the electric fluxes of C30 concrete, C40 concrete, and C50 concrete were 0.89 times, 0.67 times, and 0.53 times of C20 concrete, respectively. The electric flux decreased as the strength of concrete increased. The higher the strength of the concrete, the better the impermeability.

4 Mechanism Analysis

In order to study the internal mechanisms of concrete performance factors such as corrosion/permeability/frost resistance under different water–binder ratios, the microstructure was analyzed for different water–binder

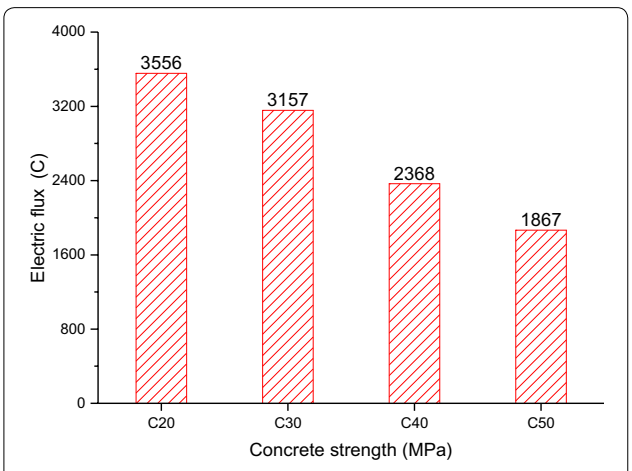

Fig. 13 Electric flux of different concrete strengths.

Table 2 The pore structure characteristic parameters of concrete.

Characteristic parameters	C20	C30	C40	C50
Porosity (%)	24.19	20.15	14.59	11.73
Pore volume (ml/g)	0.1282	0.1088	0.0900	0.0822
Pore area (m^2/g)	2.0578	7.3231	9.5481	12.1915
Specific surface area (m^2/ml)	16.0514	67.3079	81.6451	148.3150
Most probable pore diameter (nm)	151.0040	40.2913	44.3119	21.0723
Critical aperture (nm)	120.00	40.29	35.62	17.09
Average pore size (nm)	190.9	48.6	40.8	23.0

ratios and the internal causes affecting durability were then analyzed.

The total porosity of concrete decreases with increasing strength (Table 2). The total porosity values of C30 concrete, C40 concrete, and C55 concrete were 0.83 times, 0.60 times, and 0.48 times that of C20 concrete, respectively. The specific surface area of the pores increased with increasing strength. The specific surface areas of C30 concrete, C40 concrete, and C50 concrete were 4.19, 5.09, and 9.24 times that of C20 concrete, respectively. The average pore sizes of C30 concrete, C40 concrete, and C50 concrete were 0.25, 0.21, and 0.12 times that of C20 concrete, respectively. The average pore size decreased with increasing concrete strength.

Figure 14 shows that C50, C40, C30, and C20 concrete respectively accounted for 89.13%, 1.76%, 1.11%, and 0.12% of the total proportion of pores under 20 nm. C50, C40, C30, and C20 concrete respectively accounted for 53.11%, 30.30%, 26.90%, and 0.35% of the total proportion from 20 to 50 nm. C50, C40, C30, and C20 concrete respectively accounted for 3.46%, 40.94%, 42.20%, and 19.92% of the total proportion from 50 to 200 nm. C50, C40, C30, and C20 concrete respectively accounted for 4.32%, 9.24%, 7.65%, and 77.80% of the total proportion above 200 nm. The diagram visually reflects the distribution of different concrete strengths in the same pore size range. The proportion of high-strength concrete was greater in the small pore size, whereas the proportion of low-strength concrete was greater in the large pore size.

Figure 15 shows that pore diameters of less than 20 nm, 20 nm to 50 nm, 50 nm to 200 nm, and more than 200 nm were 0.03%, 0.52%, 25.11%, and 74.13% of the total pore sizes for C20 concrete, respectively, and pore diameters of less than 20 nm, 20 nm to 50 nm, 50 nm to 200 nm and more than 200 nm were 25.06%, 66.37%, 3.71%, and 4.30% of the total pore sizes for C50 concrete, respectively. The largest pore size range of C30 concrete and C40 concrete was 50 nm to 200 nm, accounting for 51.38% and 46.86% of the total pore sizes, respectively, and the second largest pore size of C30 and C40 concrete was 20 nm to 50 nm, accounting for 39.98% and 42.11% of the total pore size, respectively. It can be concluded that the higher the strength of the concrete, the less macropores were distributed, and, conversely, the lower the strength of the concrete, the more macropores were distributed. The pore size distribution demonstrates the variation rule of corrosion/permeability/frost resistance.

Figure 16 presents the differential curve of the aperture distribution. The higher the strength of concrete, the greater the chance of pores. On the contrary, the lower the strength of concrete, the greater the probability of large pores. The composition characteristics of the different samples of concrete determine that the surface and interior of the concrete structure were not dense, and there were many microcracks and pores. This internal

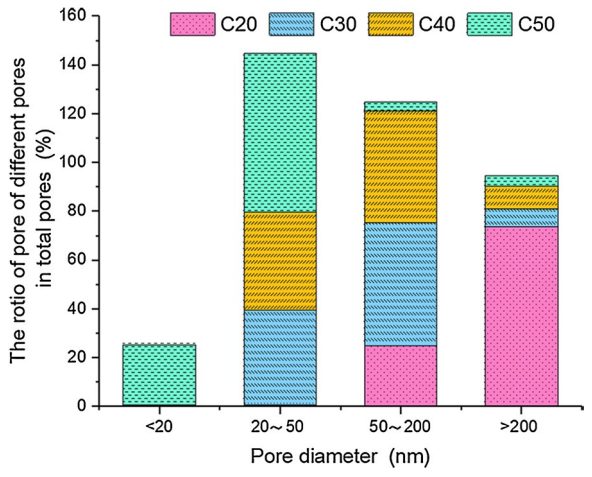

Fig. 14 Same pore diameter distribution of different concrete strengths.

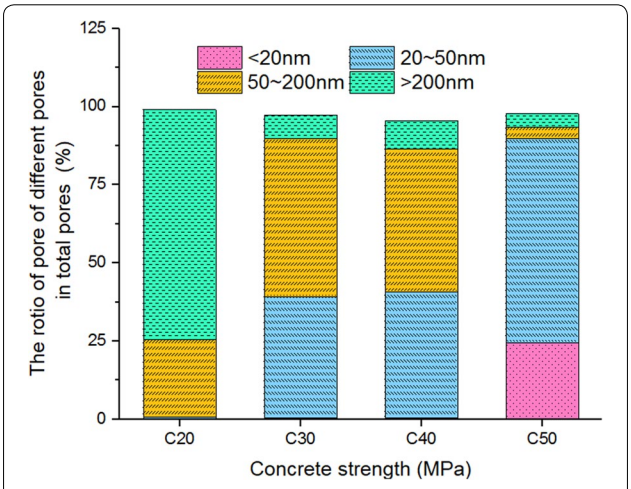

Fig. 15 Pore diameter distribution of different concrete strengths.

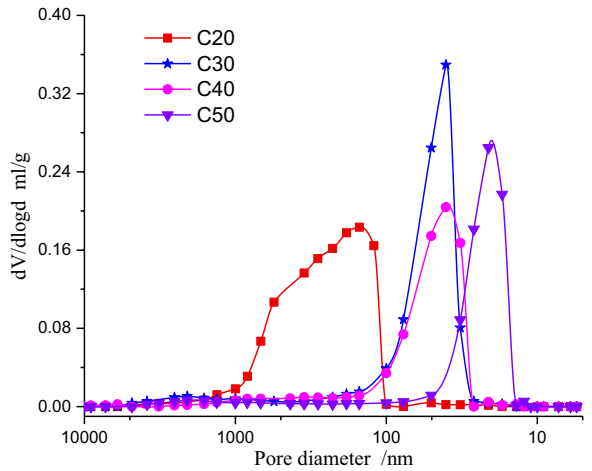

Fig. 16 Differential curve of aperture distribution.

composition structure makes damage to the concrete possible.

5 Conclusions

In this article, the corrosion, permeability, and frost resistance of concrete for different water–binder ratios were tested, and the microstructure was analyzed. The following conclusions were drawn:

- The most rapid corrosion speed was caused by dry and wet cycles, vertical semi-immersion was second, and the slowest was complete immersion among these three immersion types. Corrosion resistance decreases with increasing strength.
- The relative dynamic elastic modulus and freeze–thaw index were very sensitive to the frost resistance of concrete. These two indices are suggested to evaluate the frost resistance.
- The water–binder ratio has an obvious influence on anti-permeability: the smaller the water–binder ratio, the better the compactness of concrete and the stronger the frost resistance of concrete.
- It can be from analysis of the pore structure that the different proportions of pore sizes determine the corrosion, permeability, and frost resistance of concrete. The key to improving the durability of concrete is to change the pore structure of concrete. The smaller the pores and the more uniform their distribution, the better the durability of concrete.
- The smaller the water–binder ratio, the higher the strength and the better the corrosion, permeability, and frost resistance. In a natural environment, it is possible that a variety of factors will act together on concrete, which makes the durability of concrete more complex. Therefore, it is necessary to further carry out experimental research on the durability of concrete under the coupling of various factors.

Acknowledgements
The authors would like to express their sincere gratitude and appreciation to Lanzhou Jiaotong University and Educating Department of Gansu Provincial Government.

Authors' contributions
Conceptualization, methodology, formal analysis, investigation, resources, and data curation were performed by RZ; PL; LM; ZY; HC; HZ; HX and JL. All authors read and approved the final manuscript.

Funding
This project was sponsored by the Natural Science Foundation of China (No. 51268032), Program for Changjiang Scholars and Innovative Research Team in Lanzhou Jiaotong University (IRT_15R29), Young Elite Scientist Sponsorship Program by CAST (No. 2015142), National Natural Science Foundation of China (Grant Number 51778632), collaborative innovation team of science and technology for colleges and universities in Gansu province (2017C-08), lzjtu EP support (201606) and Longyuan Youth Innovative Talents Support Program (No. 2050205201506).

Availability of data and materials
Not applicable.

Conflicts of interests
The authors declare that they have no competing interests.

Author details
[1] School of Civil Engineering, Lanzhou Jiaotong University, Lanzhou 730070, China. [2] Cardiff School of Engineering, Cardiff University, Cardiff CF24 3AA, UK. [3] School of Civil Engineering, Central South University, 22 Shaoshan Road, Changsha 410075, China. [4] Jiangsu Key Laboratory of Construction Materials, School of Materials Science & Engineering, Southeast University, Nanjing 211189, China. [5] School of Civil Engineering, Harbin Institute of Technology, Harbin 150090, China. [6] Department of Civil, Construction, and Environmental Engineering, Iowa State University, Ames, IA 50011, USA.

Received: 19 May 2019 Accepted: 6 December 2019
Published online: 07 February 2020

References

Aye, T., & Oguchi, C. T. (2011). Resistance of plain and blended cement mortars exposed to severe sulfate attacks. *Construction and Building Materials, 25*(6), 2988–2996.

Chinese, National Standard of the People's Republic of China. (2009). *The test method of long-term and durability on ordinary concrete*. Beijing: China Architecture & Building Press.

Cho, S. W. (2012). Using mercury intrusion porosimetry to study the interfacial properties of cement-based materials. *Journal of Marine Science and Technology, 20*(3), 269–273.

D4404 ASTM. (2010). *Standard test method for determination of pore volume and pore volume distribution of soil and rock by mercury intrusion porosimetry* (p. 6). West Conshohocken, PA, USA: ASTM International.

Dehwah, H. A. F., Maslehuddin, M., & Austin, S. A. (2002). Long-term effect of sulfate ions and associated cation type on chloride-induced reinforcement corrosion in Portland cement concretes. *Cement & Concrete Composites, 24*(1), 17–25.

Du, J. M., Han, X. L., Li, Z. T., Li, G., & Ji, Y. S. (2016). Effects of water-cement ratio on concrete sulfate corrosion rate. *Key Engineering Materials, 711*, 295–301.

El Maaddawy, T., & Soudki, K. (2007). A model for prediction of time from corrosion initiation to corrosion cracking. *Cement & Concrete Composites, 29*(3), 168–175.

Gao, R., Li, Q., & Zhao, S. (2013). Concrete deterioration mechanisms under combined sulfate attack and flexural loading. *Journal of Materials in Civil Engineering, 25*(1), 39–44.
Gao, Y., & Zou, C. (2015). CT study on meso-crack propagation of gradient composite concrete subjected to sulfate erosion. *Magazine of Concrete Research, 67*(21), 1127–1134.
Hai-long, W., Yi-sen, D., Xiao-yan, S., & Wei-ling, J. (2012). Damage mechanism of concrete deteriorate by sulfate attack in wet-dry cycle environment. *Journal of Zhejiang University (Engineering Science), 46,* 1255–1260.
Haynes, H., O'Neill, R., Neff, M., & Kumar Mehta, R. (2008). Salt weathering distress on concrete exposed to sodium sulfate environment. *ACI Materials Journal, 105*(1), 35–43.
Liangxue, N., Jinyu, X. U., Yuanfei, L., Jianshe, F., & Hongwei, W. (2016). Strength change regularity and micro-structure analysis of concrete in sulfate environment. *Journal of Vibration & Shock*, *35*(20), 203–208.
Mahmoodian, M., & Alani, A. M. (2017). Effect of temperature and acidity of sulfuric acid on concrete properties. *Journal of Materials in Civil Engineering, 29*(10), 04017154.
Najjar, M. F., Nehdi, M. L., Soliman, A. M., & Azabi, T. M. (2017). Damage mechanisms of two-stage concrete exposed to chemical and physical sulfate attack. *Construction and Building Materials, 137,* 141–152.
Neville, A. (2004). The confused world of sulfate attack on concrete. *Cement and Concrete Research, 34*(8), 1275–1296.
Rao, A. S., Lepech, M. D., & Kiremidjian, A. (2017). Development of time-dependent fragility functions for deteriorating reinforced concrete bridge piers. *Structure and Infrastructure Engineering, 13*(1), 67–83.
Rozière, E., Loukili, A., El Hachem, R., & Grondin, F. (2009). Durability of concrete exposed to leaching and external sulphate attacks. *Cement and Concrete Research, 39*(12), 1188–1198.
Shaheen, F., & Pradhan, B. (2017). Influence of sulfate ion and associated cation type on steel reinforcement corrosion in concrete powder aqueous solution in the presence of chloride ions. *Cement and Concrete Research, 91,* 73–86.
Tulliani, J.-M., Montanaro, L., Negro, A., Collepardi, M. J. C., & Resdzfearch, C. (2002). Sulfate attack of concrete building foundations induced by sewage waters. *Cement and Concrete Research, 32*(6), 843–849.
Valencia Saavedra, W. G., Angulo, D. E., & Mejía de Gutiérrez, R. (2016). Fly ash slag geopolymer concrete: Resistance to sodium and magnesium sulfate attack. *Journal of Materials in Civil Engineering*, *28*(12), 04016148.
Yu, H., Tan, Y., & Yang, L. (2017). Microstructural evolution of concrete under the attack of chemical, salt crystallization, and bending stress. *Journal of Materials in Civil Engineering, 29*(7), 04017041.
Zanqun, L., Xiangning, L., Dehua, D., & Minhua, X. (2016). Comparison of paste damage in evaporation zones of portland cement paste and calcium. *Journal of the Chinese Ceramic Society, 44*(8), 1173–1177.
Zhang, W., Gong, S., & Kang, B. (2017). Surface corrosion and microstructure degradation of calcium sulfoaluminate cement subjected to wet-dry cycles in sulfate solution. *Advances in Materials Science and Engineering, 2017,* 1–8.
Zhang, M., Yang, L.-M., Guo, J.-J., Liu, W.-L., & Chen, H.-L. (2018). Mechanical properties and service life prediction of modified concrete attacked by sulfate corrosion. *Advances in Civil Engineering, 2018,* 1–7.

Publisher's Note